A study of Low Sidelobe Technology of Reflector Antenna and the Experimental Result of Decreasing its Sidelobe Level

Teruaki ORIKASA and Yoshiyuki FUJINO

For realization of STICS, a large satellite antenna is necessary. We have been studying the satellite antenna with approximately 30 m aperture size. For keeping the performance of beam shape, beam direction and sidelobe level, radiation pattern correction will be needed, because thermal distortion of reflector will be caused. In this section, radiation pattern correction experiment results are described, using developed digital beam forming network (DBF/channelizer) for studying ability of pattern correction of this DBF antenna.

1 Introduction

The essential feature of the STICS communication system is the effective utilization of frequencies through frequency reuse. To realize the system, we must address challenges such as: interference from adjacent beams caused by frequency reuse, deformation of beams (deterioration of radiation pattern) due to thermally distorted reflector in orbit, sidelobe degradation, and variations in beam direction. The proposed antenna has a reflector with 30 m class aperture diameter, so we expect that it will be folded away for launching and spread out in orbit (mesh deployable reflector antenna). Because of this, the reflector structure will not be able to avoid thermal strain when in orbit. The feeder unit of the antenna under consideration—a 100-element class phased array antenna—is controlled by a Digital Beam Former (DBF) that can deliver a high degree of freedom in controlling excitation weight. This configuration shows good potential in correcting radiation pattern deterioration.

Experiments were conducted via an earlier-developed DBF/channelizer to test for lowered sidelobe in order to create technology for realizing the potentials of low sidelobe antennae. This report describes the details and results obtained.

2 Technological considerations in achieving low sidelobe

Low sidelobe technology is classified largely into the following two types:

A: Those that incorporated measures for achieving low sidelobe at the design stage

B: Those that maintain functional integrity through corrections when experiencing radiation pattern deterioration

Technology approach A should be implemented in the design and production stages, and thus lies beyond the scope of this report. Approach B, on the other hand, focuses mainly on corrective actions against comparatively long-term variations (typically, due to thermal distortion) that occur to a large reflector antenna in orbit. This report reviews the methods involved in approach B. The satellite-mounted antenna discussed in this report—scheduled to be used in STICS—will be constructed in the same way as Experimental Test Satellite VIII (ETS-VIII). The only difference will be the adoption in the allay feeder unit of a high performance DBF Beam Forming Network (BFN), and both will employ the same type of mesh deployable reflector antenna. Therefore, they both share the problem of reflector thermal distortion. In fact, variation in beam direction was observed in ETS-VIII in orbit due to thermally distorted reflector.

ETS-VIII was launched in December 2006, and has been the platform for various communication experiments, including antenna evaluations[1][2]. In these evaluations, detailed radiation pattern measurement obtained while changing the satellite's altitude revealed that the antenna failed to fully perform to expectations. Attempts to correct this problem failed. This failure is ascribed to an inability

in sufficiently forecast the reflector's surface profile. A profile prediction experiment conducted on ETS-VIII—using the rotating element electric field vector method (REV method) supported by multiple earth stations—did not produce satisfactory results[3]. Because the largest amount of reflector distortion was 1 λ or more, it is possible that this problem was due to the unknown quantity of λ, representing the wavelength of signal.

The feeder unit under review for use in STICS is a phased array antenna mounted with a DBF, and is projected to have around 100 elements (in comparison with ETS-VIII's 31). These features are thought to endow the new antenna with a higher degree of freedom and higher corrective capabilities than that of ETS-VIII.

In this report, we will review technologies related to distortion-induced reflector radiation pattern correction. The following sections focus on three subjects in relation to measures for achieving low sidelobe.

2.1 Reflector deformation correction functions

When the reflector distorts it affects radiation pattern. To correct the radiation pattern, a corrective function must provide the capability to recalculate excitation weight corresponding to each of the distorted areas on the reflector surface. This function is indispensable in maintaining low sidelobe, and it was checked whether the DBF can perform this. Here, experiments were conducted to ascertain that the calculated values agree with the measurements. The DBF/channelizer developed for this was applied to the experiment to test its potential. Although the number of elements used in this experiment was 16, the corrective function, if proved in this experiment, is guaranteed to perform satisfactorily in the 100 elements system.

Effective reuse of frequencies presupposes lowering interference between beams sharing the same frequency. Therefore, confirmation must be made experimentally to verify that those beams that share a frequency within a specified beam sidelobe region have their level decreased in the specified direction.

2.2 RF sensor functions

RF sensors, often used as a part of a satellite-mounted multi-beam antenna, provide a function to detect angular errors in beam direction. Its main task is to detect the amount of directional variation of each beam, or variations in radiation pattern, that occur as a result of reflector distortion. The RF sensor receives a beacon signal from a ground-based beacon station and determines its incident angle accurately, and this is used to produce an angular signal output for beam direction control.

Well-calibrated beam direction means stable arrangement of beams, enabling suppression of interference between them due to positional fluctuations. In other words, misalignment of the beam direction reduces gain in the targeted area, resulting in smaller relative level differences between the beam and sidelobes. Control of beam direction is closely connected with technology for suppressing sidelobe intensity because insufficient directional control is equivalent to increased sidelobe level.

To achieve highly accurate directional control, the RF sensor has to produce sum and difference signals in a discretionary position. In this experiment, the DBF/channelizer, developed using an actual mesh reflector, was examined for potential in meeting such requirements. A simulation was also carried out to realign a miss-aligned beam with the use of a DBF/channelizer and the control computer. This effort may pave the way for automatic tracking and beam direction control provided that the RF sensor function proves capable of forming signal patterns (sum and difference).

2.3 Effect of measurement point arrangement on reflector surface profiling

As described in Subsection **2.1**, good knowledge of the reflector's surface profile enables the accurate prediction of radiation pattern and calculation of excitation weight that is needed for corrections. In concrete terms, placing targets on measurement points would be the method of choice: positional information of the targets provides keys to estimating reflector surface undulation. In practice, direct attachment of the targets on the mesh reflector surface is difficult, and the selection of target locations may be placed under certain restrictions.

To probe possibilities for forecasting reflector surface profile from the knowledge of target positions, an experimental evaluation was conducted using only a limited set of targets. One reflector, with identical inter-target distances, was used through the experiment, and measurement frequencies were varied—equivalent in effect to shifting the distances between the targets. For each measurement frequency, a matched horn antenna was used with the feeder.

3 Experiment results and discussion

This section describes and discusses the results from

the experiments on three subjects each relating to sidelobe suppression techniques. The experiments were conducted using the following combination: a mesh reflector (φ 3.3 m aperture), 16-element feeder, and DBF/channelizer. The measurements were made using the plane polar near field antenna pattern measurement facility (a facility of the Research Institute for Sustainable Humanosphere, Kyoto University)[4][5].

3.1 Reflector distortion correction experiment

(1) Outline

Distortion of the reflector gives rise to deformation in radiation pattern, resulting in skewed beam, shifted beam direction, and increasing sidelobe level. However, the radiation pattern can be corrected, taking advantage of the fact that the feeder uses a phased array antenna by controlling excitation weight of the array. To verify feasibility, experiments were conducted to correct radiation pattern by adjusting excitation weight, whereby the DBF/channelizer (developed by combining a mesh reflector and feeder) was used. Figure 1 shows the major parameters and system configuration of the antenna.

The antenna parameters are as follows: aperture D: 3.3 m, F/D: 1.04, offset angle: 37.5°. During the measurements, the array feeder was shifted 1 m away from the focal point toward the reflector (see Fig. 1). Figure 2 shows an external view of the measurement system. The Z-axis of the reflector points upward. The feeder is a 4 × 4 array, and each element consists of a patch antenna.

The DBF/channelizer is placed lower left (see the figure).

The basic objective of the experiments was to compare reflector surface in a normal state and in a deliberately distorted state. Figure 3 shows the flow of testing steps. In the first step, measurements were made of the original reflector shape. In this step, a photographic measurement system—V-STARS from company Geodetic Systems, Inc. (GSI)—was used for locating the exact position of the targets.

Figure 4 shows an external view of the reflector and targets (white points in the figure indicate the targets attached to the reflector surface).

The targets in the figure look especially bright because they reflected the light of the flash photography used. Figure 5 shows a scene during the photographic measurement session. Photographs were taken from above from various angles from a crane.
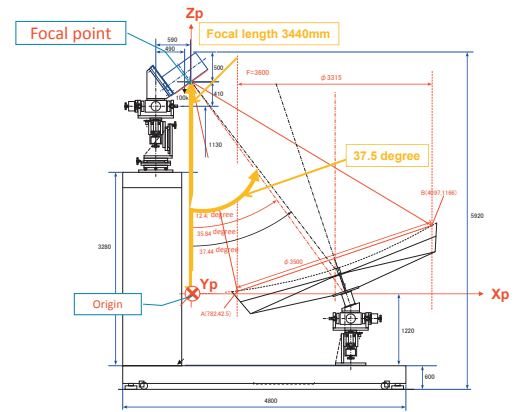
After completing original shape measurements, radia-

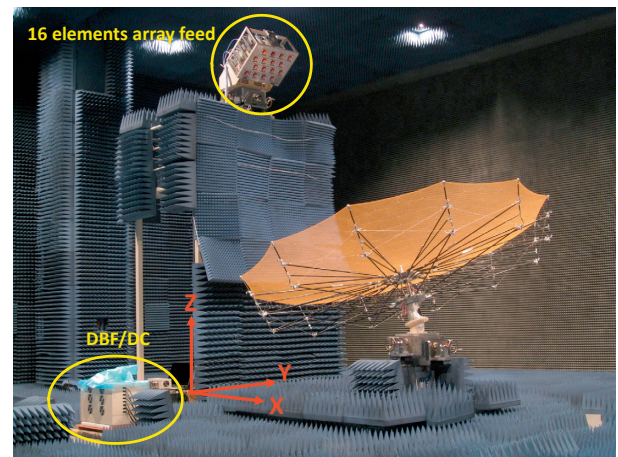**Fig. 1** Parameter of measured antenna
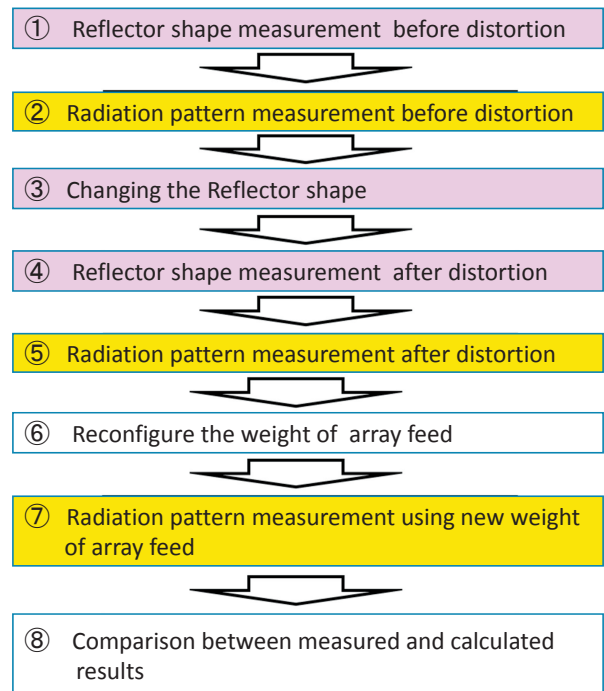

Fig. 2 Outline view of measurement

① Reflector shape measurement before distortion

② Radiation pattern measurement before distortion

③ Changing the Reflector shape

④ Reflector shape measurement after distortion

⑤ Radiation pattern measurement after distortion

⑥ Reconfigure the weight of array feed

⑦ Radiation pattern measurement using new weight of array feed

⑧ Comparison between measured and calculated results

Fig. 3 Experiment flow of correction of reflector distortion

Fig. 4 Mesh reflector and target

Fig. 5 Measurement of reflector shape
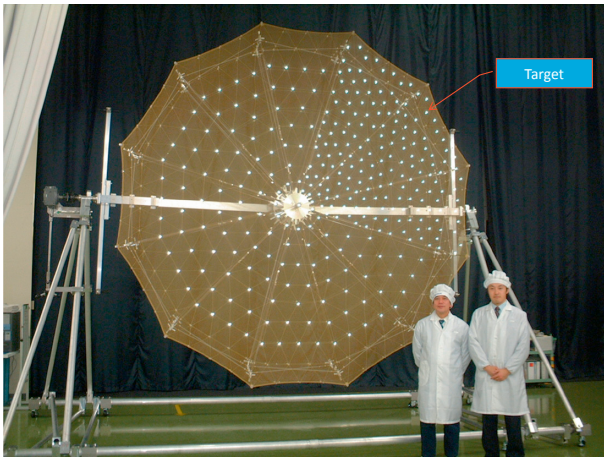
Fig. 6 View of distorted mesh using weight
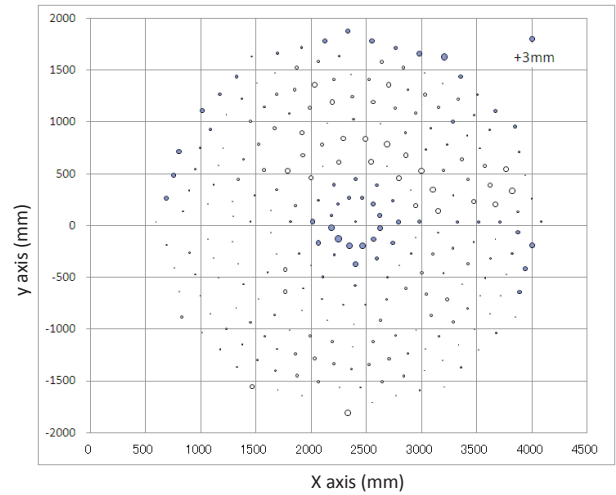
Fig. 7 Error of normal reflector surface
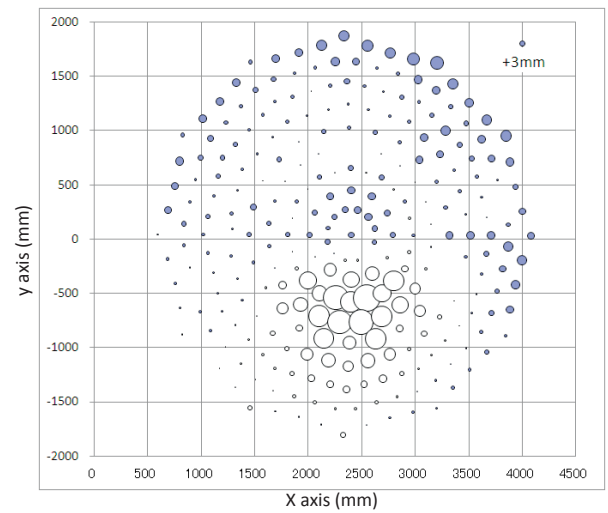
Fig. 8 Error of distorted reflector surface

the surface profile in the same way as step 1. Figure 7 represents the surface profile before the artificial distortion process, and Fig. 8 after. Circles in the figures show the level of deviation from ideal shape: the larger the circle, the greater the deviation. Coloring of the circles indicate the direction of deviation: blue indicates upward (Z-axis) deviation and white downward. The large white circles in Fig. 8 represent the locations that suffered distortion.

Following the reflector profile measurements, pattern measurements were conducted in step 5.

Plane polar neat-field antenna measurement equipment was used for the pattern measurements. With the normal reflector surface, shown in Fig. 7, the largest deviation projecting forward from the flat face in contrast to ideal parabola was only 3 mm, and most deviation areas did not exceed 1 mm. In contrast, a distorted reflector surface (Fig. 8) showed deviation as large as 15 mm projecting

tion pattern was measured in step 2. Radiation pattern was measured with the floor and fixtures covered by radiowave absorber sheets (see Fig. 2). Next comes the distortion of the reflector in step 3. As shown in Fig. 6, bolts were suspended from the rear surface of the mesh reflector, exerting downward force to create distortion.

After distorting the reflector, step 4 was to re-measure

away (white circles), indicating clearly the distorting effect of the suspended bolts.

Figure 9 shows the configuration of the measurement system. A receiver antenna was used in this experiment. A CW signal was radiated from the probe (see Fig. 9), reflected by the reflector, and received by the feeder. The signal is recorded by the measurement system after passing through an Rx DBF/channelizer. As the floor on which the system (reflector, feeder, DBF/channelizer) is installed rotates, signals are delivered to the measurement system after passing through a rotary joint embedded on the floor. The probe of the measurement system scans in a uniaxial (radial) direction.

The range of the scan is shown in Fig. 10, in relation to the installations. The scan range forms a circle with a diameter of approx. 7 m.

A comparative evaluation is made between the data from the pattern measurement (step 5) and that obtained from the undistorted reflector. Based on this evaluation, new excitation weight is calculated in step 6 to correct the

distorted radiation pattern. A new pattern measurement is done using the new excitation weight setting (step 7) for evaluation of this correction method.
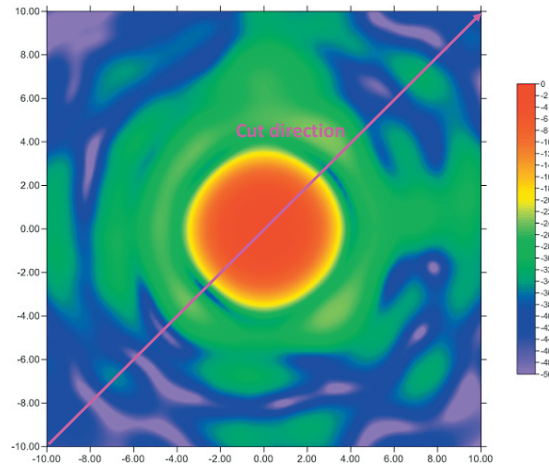

Fig. 11   Radiation pattern of nominal shape reflector (measured value)
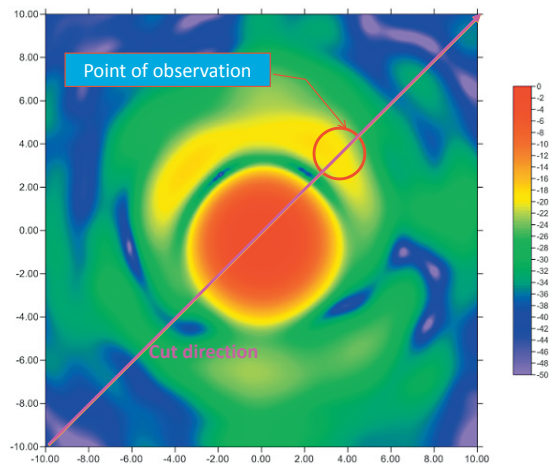
Fig. 12   Radiation pattern of distorted shape reflector (measured value)

Fig. 9   Configuration of sidelobe re-forming experiment for reflector distortion effect

Fig. 10   Scan area for pattern measurement

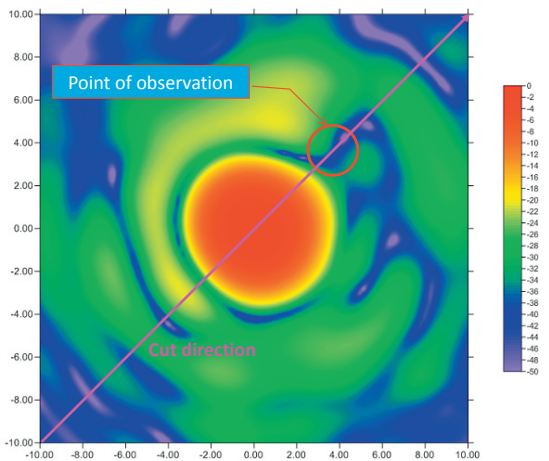
Fig. 13   Re-formed radiation pattern (measured value)

(2) Test results

Pre- and post-distortion radiation patterns are shown in Fig. 11 and Fig. 12 respectively. As is apparent from the post-distortion radiation pattern, sidelobe level has increased (see the point tabbed "note here" in the figure).

Figure 13 shows the radiation pattern measured after excitation weight correction. Excitation weight was calculated by giving a low level constraint point to suppress intensity of the sidelobe. It was found that the level of the sidelobe at the point ("note here") decreased.

To explain more clearly, the patterns of the views will be explained here. The patterns are those shown in the cross section pictures of Figs. 11 to 13. Figure 14 shows a cross-sectional radiation pattern for the non-distorted (normal) reflector with nominal variation. The right-hand side of the figure shows the region of the first sidelobe that was tested in the experiment. The red line represents the measured radiation pattern, and the blue line is the calculated plot line that was projected based on reflector profile measurements.

The first sidelobe has an intensity level of approximately -25 dB. Figure 15 shows the radiation pattern after the reflector underwent artificial distortion. Intensity of the first sidelobe has risen to the level of approximately -18 dB.

Figure 16 shows the results of radiation pattern measurement after corrective procedures—calculation and application of excitation weight based on the distorted reflector to reduce the sidelobe level in the section indicated by the arrow. It was found that levels dropped for the section being observed.

As a result of the experiments, it was found that even with a 16-array setup it is possible, if profile deviation information is available, to make corrections by lowering the sidelobe level even if the reflector surface is deformed.

3.2 RF sensor function verification

RF sensor function can be verified if it can establish a null pattern on an actual reflector surface. The measurement system used for this experiment has the same configuration as that used for the error correction experiment (see Fig. 9). In terms of RF sensors, normal radiation pattern is called a sum signal (E_Σ), and the radiation pattern for angular error is called a difference signal (E_Δ). The difference signal outputs elevation and azimuth errors relative to the normal angular direction.

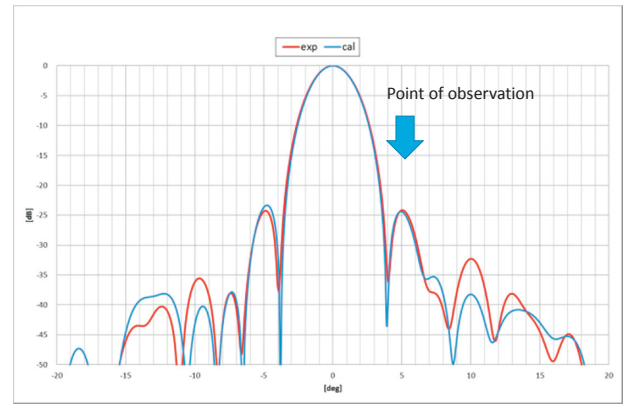Figure 17 shows the results of null-pattern measurement for RF sensors. Two radiation patterns are created:

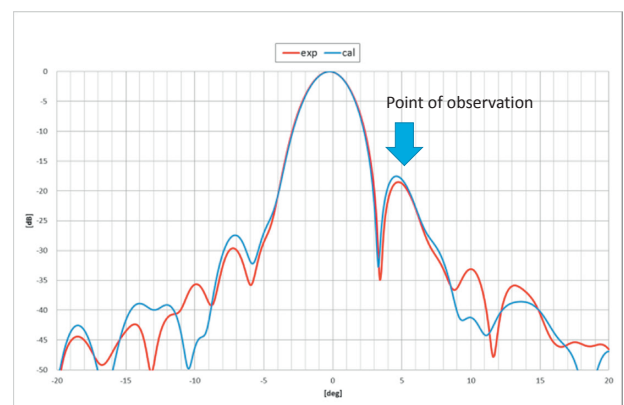
Fig. 14 Cut pattern of nominal shape reflector

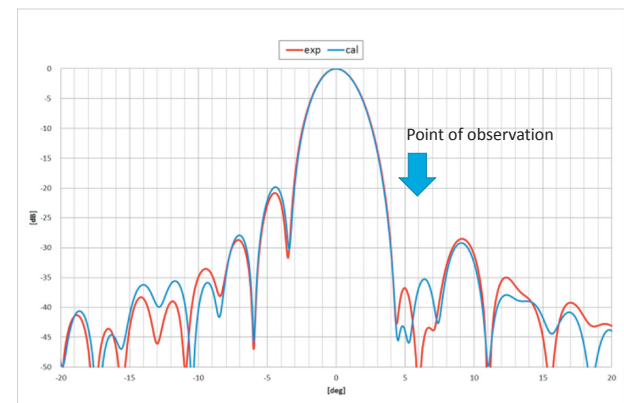**Fig. 15** Cut pattern of distorted shape reflector

Fig. 16 Cut pattern of re-formed sidelobe pattern (measured value)

one for elevation and the other for azimuth. Here, the elevation and azimuth plane correspond respectively to the z_P-x_P plane and the y_P-z_P plane of Fig. 1. As shown in Fig. 17, distribution of null points typically forms a channel-like shape. The elevation pattern has good vertical symmetry, while the azimuth error pattern does not show very good symmetry. This deviation has its origin in the feeder arrangement: as shown in Fig. 18, the elements are arranged in an asymmetric manner from right to left (relative to
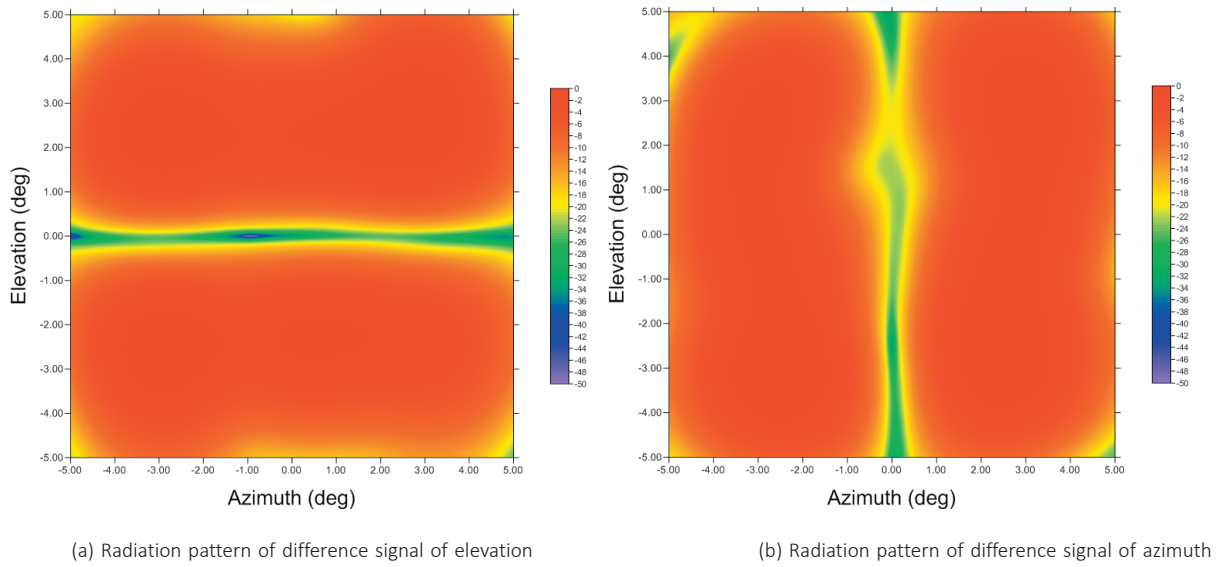
(a) Radiation pattern of difference signal of elevation

(b) Radiation pattern of difference signal of azimuth

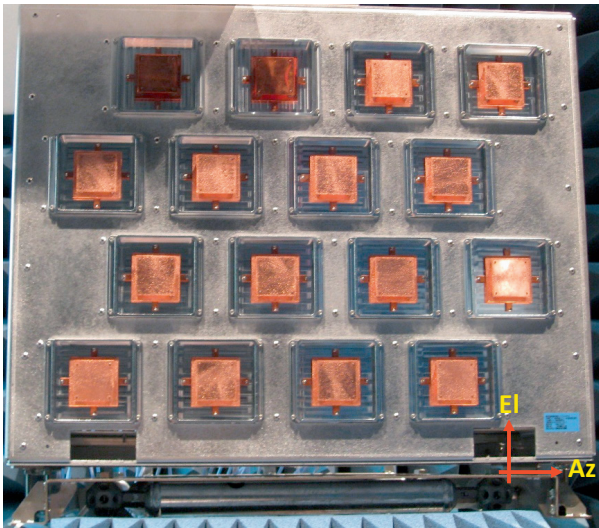**Fig. 17** Radiation pattern of difference signal

Fig. 18 Configuration of 16 elements array feed

azimuth direction). The low element count of only 16 and the small degree of freedom also has an effect. It is thought that more symmetric patterns will become obtainable as the number of elements increases.

Figure 19 shows cross-sectional patterns along the elevation direction. The red line represents measured data, and the blue plot line represents the projected levels. As seen in the figure, a null point is generated at the center. To cope with variations in input power, the signal is normalized using the sum signal. Consequently, signal level of angular error is expressed as:

Angular error: $\delta E = \dfrac{E_\Delta}{E_\Sigma}$ (1)

δE becomes larger as the angular error increases.

Experiments were conducted in an attempt to form radiation patterns for RF signal using an actual mesh reflector, and the results of which confirmed feasibility of RF sensor pattern formation.

### 3.3 Experiments on target intervals

Reflector surface measurements require a set of defined measurement points on the surface. In the case of the measurement using V-STARS, a set of targets must be arranged. Figure 4 shows with white points the arrangement of targets on the surface of the actual reflector used for the measurement. Figure 20 is an expanded view, showing some of the targets surrounded by red circles.

These are the measurement hard points on the reflector. The arrows shown in yellow are pointing out the targets attached to the reflector surface. Although a part of this reflector allows target attachment in this way, actual satellite-mounted reflectors do not permit such a method. The targets are attached at an interval of approximately 200 mm (except for within the mesh).

In view of gaining highly accurate pattern calculations, horn antennas with known characteristics were used in the measurements. Figure 21 shows the installation of a S-band horn. The horn was mounted on the focal point of the system (see Fig. 1).

The configuration of the measurement system is shown in Fig. 22.

Experiments were conducted using the following three frequencies:
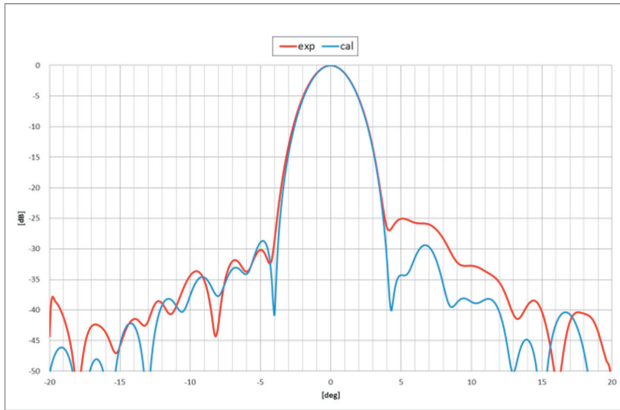
(a) Sum signal pattern (direction of elevation)
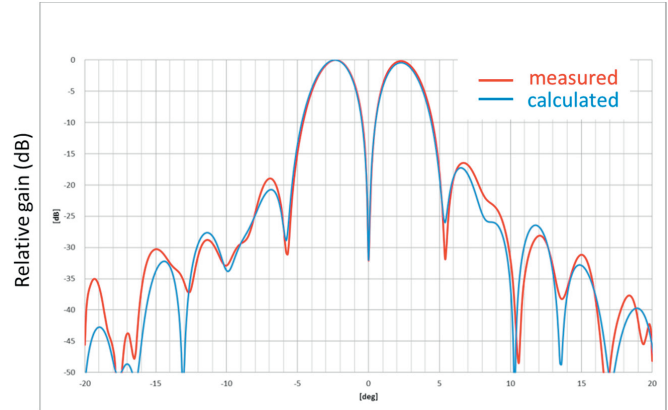
(b) Difference signal pattern (direction of elevation)

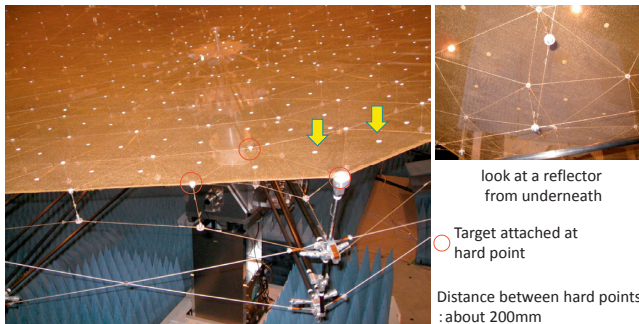**Fig. 19** Cut pattern of RF-sensor
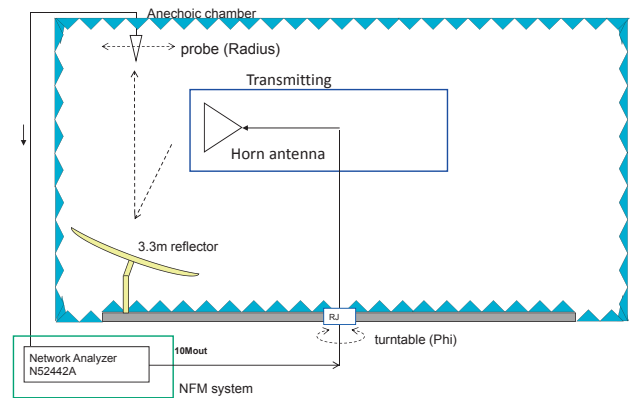

Fig. 20 Mesh reflector and target

Fig. 21 General view of measurement configuration of reflector antenna using S band horn antenna

Fig. 22 Configuration of pattern measurement experiment for effect of target space

S band: 1995.1 GHz

X band: 11.0 GHz (× 5.5 interval)

Ka band: 20.0 GHz (× 10 interval)

The results of the measurements are shown in Figs. 23, 24, and 25. The red plot lines represent measured data, and the blue lines plot calculations. These figures indicate good agreement between measured and calculated data around

boresight even in higher frequencies. In view of the fact that higher frequencies means larger equivalent dimensions, the figures also indicate the effectiveness of this evaluation method at larger measurement intervals, especially around boresight. Although the physical target interval used in this experiment was 200 mm, its equivalent distance becomes ten times larger (2,000 mm) if Ka band is used for the measurements. Slow undulations of reflector surface become dominant as the measurement interval becomes wider, and it is thought that this will allow evaluation of radiation patterns around boresight. In contrast, in wide field regions where rapid up-and-down behavior becomes dominant, there is an increase in the deviation of measured data from that projected. To enhance accuracy of radiation pattern prediction in wide field regions, supplementary techniques are needed to interpolate the surface shape between the measurement points.
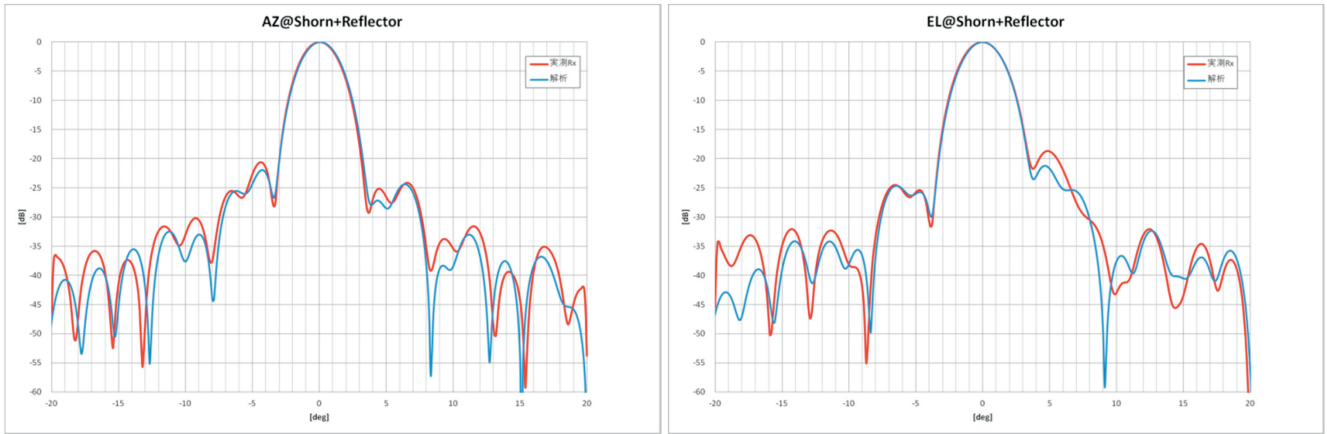
(a) Cut pattern (YZ-Plane)　(Az direction)

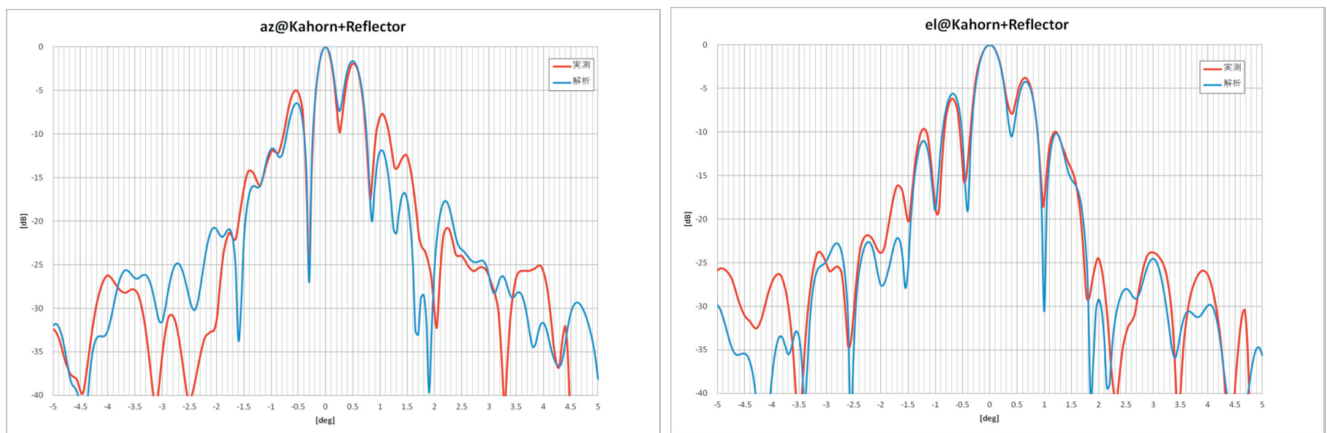(b) Cut pattern(XZ-Plane)　(El direction)

Fig. 23　Radiation pattern　using　S band horn feed
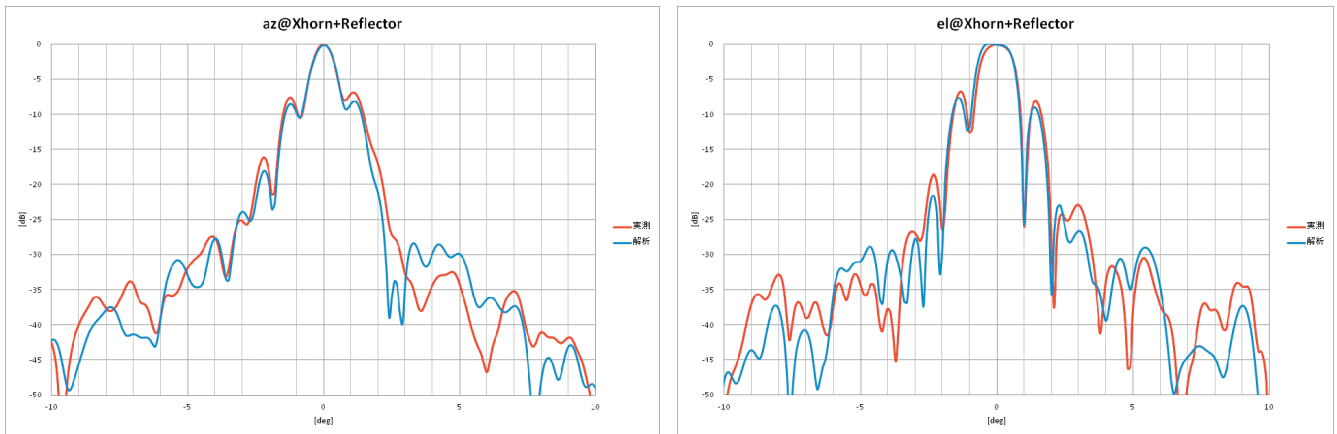
(a) Cut pattern(YZ-plane)　(Az direction)

(b) Cut pattern(XZ-plane)　(El direction)

Fig. 24　Radiation pattern　using　X band horn feed

(a) Cut pattern(YZ-plane)　(Az direction)

(b) Cut pattern(XZ-plane)　(El direction)

Fig. 25　Radiation pattern　using　Ka band horn feed

4   Conclusion

With a view to future establishment of the sidelobe suppression technology required in constructing large scale antennas, experiments were conducted in an attempt to correct radiation pattern in a distorted reflector by suppressing sidelobe level through the use of a DBF/channelizer. In the experiments, an actual mesh reflector was distorted and served for radiation pattern measurements and surface profile prediction (calculation). Based on this data, excitation weight distribution for the array antenna was reconfigured to correct the radiation pattern. The results clearly indicated the feasibility of correcting deformed radiation pattern caused by reflector distortion. In terms of directional variations in the beam, this study confirmed the feasibility of constructing RF sensor patterns on an actual mesh reflector surface. The experiments carried out using different frequencies and different equivalent measurement intervals indicated the feasibility of acceptable radiation pattern evaluation around boresight even with wide measurement intervals. For wide field regions, however, it became apparent that further information is needed to interpolate reflector surface profile between the measurement points. To ensure creation of stable radiation pattern from the antenna in orbit, the following techniques need to be developed in the future: methods for measuring reflector surface profile in orbit, and, methods for predicting surface shape between the measurement points.

5   Acknowledgments

References

1   M. Satoh, Y. Fujino, and T. Orikasa, "Characterization of Large-Scale Deployable Antenna Pattern Equipped with Engineering Test Satellite VIII on Orbit," Trans IEICE on Communications (Japanese edition), Vol.J91-B, No.12, pp.1641–1643, Jan. 2008.

2   M. Satoh, T. Orikasa, and Y. Fujino, "Evaluation of Electrical performance for Large-Scale Deployable Reflector Antenna Equipped with Engineering Test Satellite VIII on Orbit," Trans IEICE on Communication (Japanese edition), Vol.J94-B, No.3, pp.344–352, Jan. 2011.

3   T. Orikasa, M. Satoh, S. Yamamoto, and K. Kawasaki, "Error Correction Experiment of Radiation Pattern of Large Reflector Antenna," Special issue of this NICT Journal, Vol.61, No.1, 2014.

4   T. Orikasa, Y. Fujino, M. Satoh, and H. Tsuji, "Measurement experiment and evaluation of radiation patterns of the mesh reflector antenna mounted on communication satellite for hybrid mobile communication system," 63rd International Astronautical Congress, IAC-12-B2.2.6, Oct. 2012.

5   T. Orikasa, Y. Fujino, and H. Tsuji, "Experiment of satellite antenna with reflector and DBF/channelizer for STICS," IEICE Technical Report (Japanese edition), WPT-2012-45, May 2013.

Teruaki ORIKASA, Dr. Eng.

Senior Researcher, Spacre Communication Systems Laboratory, Wireless Network Research Institute
Space Communication, Antenna

Yoshiyuki FUJINO, Dr. Eng.

Professor, Department of Electrical and Electronic Engineering, Faculty of Science and Engineering, Toyo University/Former: Senior Researcher, Space Communication Systems Laboratory, Wireless Network Research Institute (–April 2013)
Satellite Communication, Antenna, Wireless Power Transmission